THE EUROPEAN
PHYSICAL JOURNAL C

A new evaluation of the hadronic vacuum polarisation contributions to the muon anomalous magnetic moment and to $\alpha(m_Z^2)$

M. Davier[1], **A. Hoecker**[2], **B. Malaescu**[3], **Z. Zhang**[1,a]

[1] Laboratoire de Physique des 2 Infinis Iréne Joliot-Curie, Université Paris-Saclay et CNRS/IN2P3, Orsay, France
[2] CERN, 1211, Geneva 23, Switzerland
[3] LPNHE, Sorbonne Université, Paris Diderot Sorbonne Paris Cité, CNRS/IN2P3, Paris, France

Abstract We reevaluate the hadronic vacuum polarisation contributions to the muon magnetic anomaly and to the running of the electromagnetic coupling constant at the Z-boson mass. We include newest $e^+e^- \to$ hadrons cross-section data together with a phenomenological fit of the threshold region in the evaluation of the dispersion integrals. The precision in the individual datasets cannot be fully exploited due to discrepancies that lead to additional systematic uncertainty in particular between BABAR and KLOE data in the dominant $\pi^+\pi^-$ channel. For the muon $(g-2)/2$, we find for the lowest-order hadronic contribution $(694.0 \pm 4.0) \cdot 10^{-10}$. The full Standard Model prediction differs by 3.3σ from the experimental value. The five-quark hadronic contribution to $\alpha(m_Z^2)$ is evaluated to be $(276.0 \pm 1.0) \cdot 10^{-4}$.

1 Introduction

The Standard Model (SM) predictions of the anomalous magnetic moment of the muon, $a_\mu = (g_\mu - 2)/2$, with g_μ the muon gyromagnetic factor, and of the running electromagnetic coupling constant, $\alpha(s)$, an important ingredient of electroweak theory, are limited in precision by hadronic vacuum polarisation (HVP) contributions. The dominant hadronic terms can be calculated with the use of experimental cross-section data, involving e^+e^- annihilation to hadrons, and perturbative QCD to evaluate energy-squared dispersion integrals ranging from the $\pi^0\gamma$ threshold to infinity. The kernels occurring in these integrals emphasise low photon virtualities, owing to the $1/s$ descent of the cross section, and, in case of a_μ, to an additional $1/s$ suppression. About 73% of the lowest order hadronic contribution to a_μ and 58% of the total

uncertainty-squared are given by the $\pi^+\pi^-(\gamma)$ final state,[1] while this channel amounts to only 12% of the hadronic contribution to $\alpha(s)$ at $s = m_Z^2$ [1].

In this work, we reevaluate the lowest-order hadronic contribution, $a_\mu^{\mathrm{had,LO}}$, to the muon magnetic anomaly, and the hadronic contribution, $\Delta\alpha_{\mathrm{had}}(m_Z^2)$, to the running $\alpha(m_Z^2)$ at the Z-boson mass using newest $e^+e^- \to$ hadrons cross-section data and updated techniques. In particular, we perform a phenomenological fit to supplement less precise data in the low-energy domain up to 0.6 GeV. We also reconsider the systematic uncertainty in the $\pi^+\pi^-$ channel in view of discrepancies among the most precise datasets.

All the experimental contributions are evaluated using the software package HVPTools [2]. To these are added narrow resonance contributions evaluated analytically, and continuum contributions computed using perturbative QCD.

2 Combination of experimental inputs

The integration of data points belonging to different experiments with their own data densities requires a careful treatment to avoid biases and to properly account for correlated systematic uncertainties within the same experiment and between different experiments, as well as within and between different channels. Quadratic interpolation (splines) of adjacent data points is performed for each experiment, and a local combination in form of a weighted average of the interpolations is computed in bins of 1 MeV, or in narrower bins for the ω and ϕ resonances.

---

a e-mail: zhangzq@lal.in2p3.fr (corresponding author)

---

[1] Throughout this paper, final state photon radiation is implied for all hadronic final states.

The uncertainties on the combined dataset, the data integration and the phenomenological fit are computed using large numbers of pseudo-experiments. These are generated taking into account all measurement uncertainties and their correlations. While this treatment guarantees a proper propagation of uncertainties, the resulting precision of the combination still depends on the chosen test statistic: a poor choice (e.g., an arithmetic instead of a weighted average) would lead to poor precision, while an aggressive choice (e.g., exploiting the available correlation information globally over the full spectrum, thereby benefiting from constraints among different energy regimes[2]) could lead to an optimistic precision claim with the risk of undercoverage with respect to the (unknown) truth. To avoid either case, we employ a test statistic that only relies on local measurement uncertainties and correlations to combine datasets in a given bin.[3] As stated above, the uncertainty in each combined bin and the correlation among bins are evaluated using pseudo-experiments generated with the full correlation information. Correlations between channels are accounted for by propagating individually the common systematic uncertainties.[4]

Where results from different datasets are locally inconsistent, the combined uncertainty is rescaled according to the local χ^2 value and number of degrees of freedom following the PDG prescription [6]. Such inconsistencies are currently limiting the precision of the combination in the dominant $\pi^+\pi^-$ channel as well as in the K^+K^- channel (see discussions below). In most exclusive channels the largest weight in the combination is provided by BABAR data.

Closure tests with known distributions have been performed in the dominant $\pi^+\pi^-$ channel to validate both the combination and integration procedures.

3 Input data

Exclusive bare hadronic cross-section measurements for 32 channels are integrated up to 1.8 GeV over the relevant dispersion kernels. This analysis uses all the available public data with recent additions [7–16]. References for data already included in our 2017 analysis are provided in the corresponding paper [1] as well as earlier publications [17–19].

In the energy range 1.8–3.7 GeV and above 5 GeV four-loop perturbative QCD is used [20]. The contributions from the open charm pair production region between 3.7 and 5 GeV are again computed using experimental data. For the narrow resonances J/ψ and $\psi(2S)$ Breit–Wigner line shapes are integrated using their currently best known parameters [6].

The following discussion of individual channels focuses on the HVP contribution to a_μ as it relies more strongly on the low-energy experimental data. We mainly explore the impact of the data released since our last publications [1,17]. If not stated otherwise, all numerical results for a_μ are quoted in units of 10^{-10}.

3.1 The $\pi^+\pi^-$ channel

Data from the BABAR [21,22] and KLOE [23–25] experiments dominate the measurement of the $\pi^+\pi^-$ channel. Their sub-percent precision is not matched by the other experiments (CMD-2, SND, and BESIII[5]). New data in this channel stem from CLEO [10] using large angle initial state radiation (ISR) and taking into account up to one additional photon, following the BABAR method [22]. Relatively large statistical uncertainties and a systematic uncertainty of 1.5% are, however, insufficient to improve the precision of the combined $\pi^+\pi^-$ contribution. Recently, a combination of the three KLOE measurements was proposed [27]. We do not use this combination as the KLOE measurements correspond to different ISR topologies and normalisation procedures.[6]

---

[2] Systematic uncertainties are based on estimates which are impacted by imponderables regarding size and correlation among measurements, in particular uncertainties due to theoretical modelling. Systematic uncertainties are often evaluated in relatively wide mass ranges, the event topology may evolve between measurements performed at different centre-of-mass energies (affecting for example the acceptance and tracking efficiency) as does the background composition, systematic uncertainties due to trigger and tracking may be correlated, etc. It is therefore important to treat systematic uncertainties and their correlations with care and avoid the use of long-range correlations to constrain measurements among different centre-of-mass energies. Ambiguities in systematic uncertainties and their correlations have been studied in other experimental areas and different "configurations"/"scenarios" of uncertainties were proposed [3–5].

[3] This information on the uncertainties and correlations is used on slightly wider ranges, of typically up to a couple of 100 MeV, when *averaging regions* are defined in order to account for the difference between the point-spacing and bin-sizes for the various experiments [2]. In this procedure the systematic uncertainties are not constrained, but rather directly propagated from each input measurement to the *averaging regions* and then to the fine bins.

[4] A number of 15 such uncertainties are accounted for in the current study. Typical examples are the luminosity uncertainties, if the data stem from the same experimental facility but measure different channels, and uncertainties related to radiative corrections.

[5] There is a small inconsistency between the bin-by-bin statistical uncertainties and the diagonal values of the statistical covariance matrix of the $\pi^+\pi^-$ data published by BESIII [26].

[6] Using the KLOE combination [27] we find for $a_\mu^{\text{had,LO}}[\pi\pi]$ between the $\pi^+\pi^-$ threshold and 1.8 GeV a value of 506.6 ± 2.4, which is to be compared with 506.7 ± 2.3 as obtained from the HVPTools combination. For both calculations the usual local $\sqrt{\chi^2/\text{ndof}}$ uncertainty rescaling method was applied. Without the rescaling the corresponding results are 506.6 ± 2.0 and 506.7 ± 2.0, respectively. The similarity of the results is maintained when using a phenomenological fit up to 0.6 GeV (see later in text).
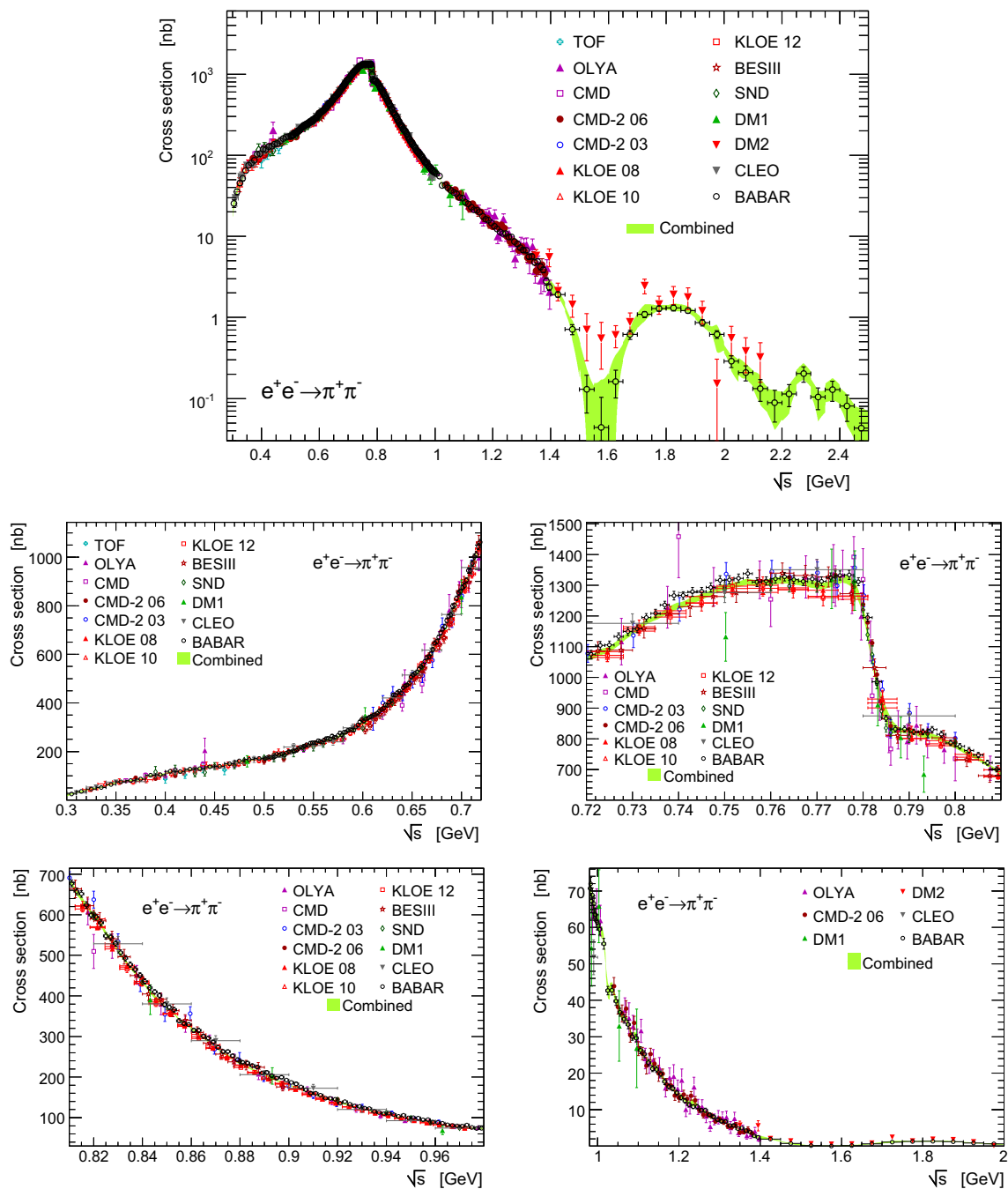
Fig. 1 Bare cross section of $e^+e^- \to \pi^+\pi^-$ versus centre-of-mass energy for different energy ranges. The error bars of the data points include statistical and systematic uncertainties added in quadrature. The green band shows the HVPTools combination within its 1σ uncertainty

Eigenvector decomposition of the statistical and systematic covariance matrices of the three most recent series of KLOE measurements [27] is used. Each eigenvector multiplied by the square-root of the corresponding eigenvalue is treated as an uncertainty source that is fully correlated between the KLOE data points, while the individual sources are treated as independent among each other. Pseudo-experiments are gen-

erated in the usual way to propagate correlated uncertainties among the KLOE measurements.

Figure 1 shows the available $e^+e^- \to \pi^+\pi^-$ cross-section measurements in various panels zooming into different energy ranges. The green band indicates the HVPTools combination within its 1σ uncertainty. Comparisons between the combination and the most precise individual measurements are plotted in Fig. 2. Figure 3 (left) shows the local
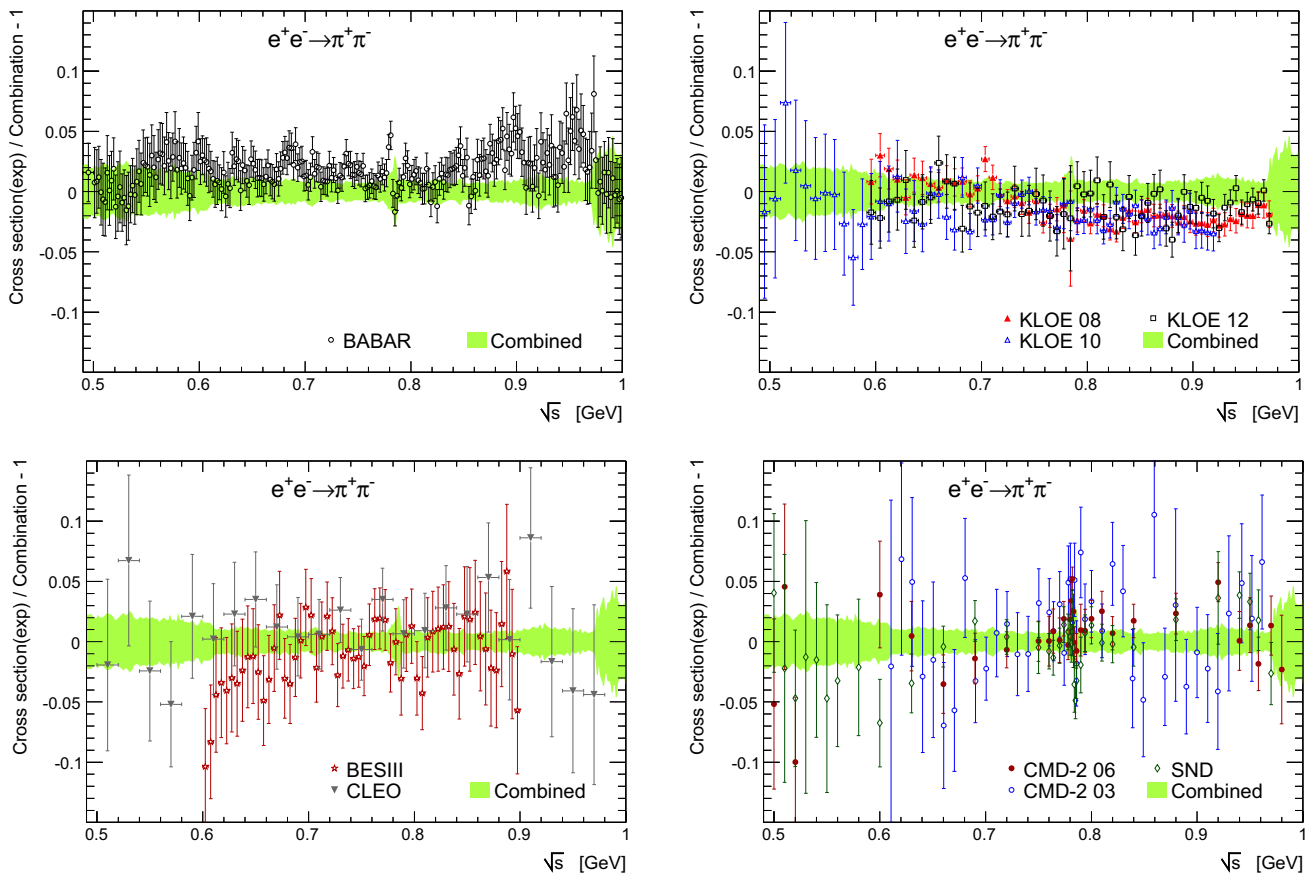
Fig. 2 Comparison between individual $e^+e^- \to \pi^+\pi^-$ cross-section measurements from BABAR [21,22], KLOE 08 [23], KLOE 10 [24], KLOE 12 [25], BESIII [26], CLEO [10], CMD-2 03 [28], CMD-2 06 [29–31], SND [32], and the HVPTools combination. The error bars include statistical and systematic uncertainties added in quadrature
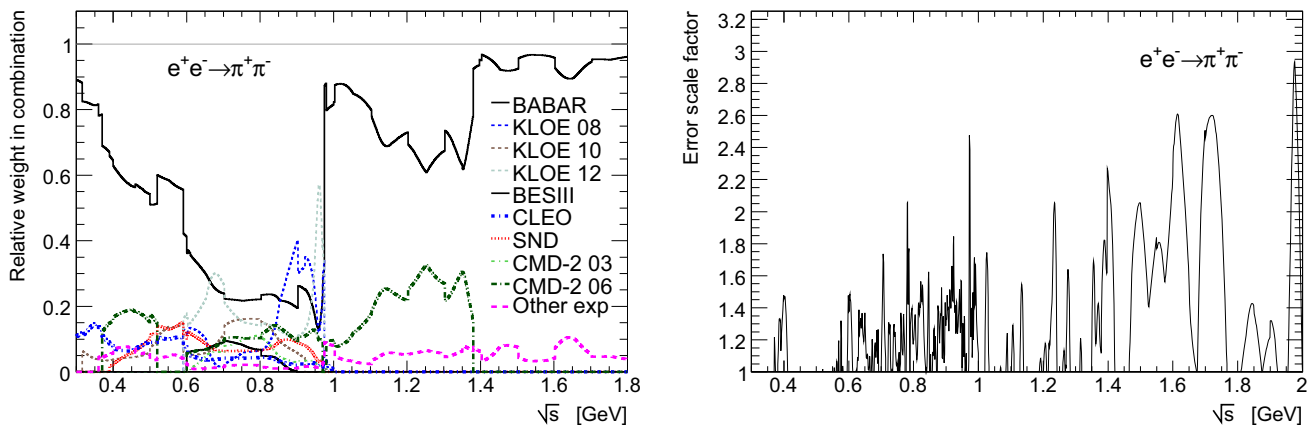

Fig. 3 Left: relative local weight per experiment contributing to the $e^+e^- \to \pi^+\pi^-$ cross-section combination versus centre-of-mass energy. Right: local scale factor versus centre-of-mass energy applied to the combined $\pi^+\pi^-$ cross-section uncertainty to account for inconsistency in the individual measurements

combination weight versus $\sqrt{s}$ per experiment. The BABAR and KLOE measurements dominate over the entire energy range. Owing to the sharp radiator function, the KLOE event yield increases towards the $\phi(1020)$ mass leading to a better

precision than BABAR in the 0.8–1.0 GeV region. The group of experiments labelled "Other exp" in the left panel of Fig. 3 corresponds to older data with incomplete radiative corrections. Their weights are small throughout the entire energy

Table 1 Results of the fit to all $\pi^+\pi^-$ data. The diagonal elements give the fitted parameter values and their uncertainties, while the off-diagonal elements give the correlation coefficients

	α_V	$\kappa[10^{-4}]$	B_0	B_1	m_ρ [MeV]	m_ω [MeV]
α_V	0.133 ± 0.020	0.52	-0.45	-0.97	0.90	-0.25
κ [10^{-4}]		21.6 ± 0.5	-0.33	-0.57	0.64	-0.08
B_0			1.040 ± 0.003	0.40	-0.40	0.29
B_1				-0.13 ± 0.11	-0.96	0.20
m_ρ [MeV]					774.5 ± 0.8	-0.17
m_ω [MeV]						782.0 ± 0.1

domain. The right hand panel of Fig. 3 shows the scale factor versus centre-of-mass energy that is locally applied to the combined $\pi^+\pi^-$ cross-section uncertainty to account for inconsistencies among the individual measurements. Significant inconsistencies are found between the most precise BABAR and KLOE datasets.

The computation of the dispersion integral over the full $\pi^+\pi^-$ spectrum requires to extend the available data to the region between threshold and 0.3 GeV, for which we use a fit as described below.

Phenomenological fit

The bare $e^+e^- \to \pi^+\pi^-$ annihilation cross section is related to the pion form factor $F_\pi^0(s)$ (excluding vacuum polarisation) by

$$\sigma^{(0)}(e^+e^- \to \pi^+\pi^-) = \frac{\pi\alpha^2}{3s}\beta_0^3(s) \cdot |F_\pi^0(s)|^2 \cdot \text{FSR}(s),$$
(1)

where α is the electromagnetic coupling constant, $\beta_0(s) = \sqrt{1 - 4m_\pi^2/s}$ is a threshold kinematic factor and FSR(s) is the final state radiation contribution.

The pion form factor is an analytic function of s in the complex plane, except on the real axis above $4m_\pi^2$. It can be parameterised as a product of two functions [33]

$$F_\pi^0 = G(s) \cdot J(s)$$
(2)

where

$$G(s) = 1 + \alpha_V s + \frac{\kappa s}{m_\omega^2 - s - im_\omega\Gamma_\omega},$$
(3)

and, exploiting the unitarity constraint which identifies $\arg(F_\pi^0)$ with the P-wave $\pi^+\pi^-$ phase shift $\delta_1(s)$,

$$J(s) = e^{1-\delta_1(s_0)/\pi} \cdot \left(1 - \frac{s}{s_0}\right)^{\left[1-\frac{\delta_1(s_0)}{\pi}\right]\frac{s_0}{s}} \left(1 - \frac{s}{s_0}\right)^{-1}$$

$$\cdot \exp\left(\frac{s}{\pi}\int_{4m_\pi^2}^{s_0} dt \frac{\delta_1(t)}{t(t-s)}\right).$$
(4)

The last term in Eq. (3) accounts for $\rho - \omega$ mixing. The function $J(s)$ is taken from Refs. [34,35]. Owing to ρ dominance, the phase shift $\delta_1(s)$ can be parameterised by [36]

$$\cot\delta_1(s) = \frac{\sqrt{s}}{2k^3(s)}\left(m_\rho^2 - s\right)\left(\frac{2m_\pi^3}{m_\rho^2\sqrt{s}} + B_0 + B_1\omega(s)\right)$$
(5)

with

$$k(s) = \frac{\sqrt{s - 4m_\pi^2}}{2}, \quad \omega(s) = \frac{\sqrt{s} - \sqrt{s_0 - s}}{\sqrt{s} + \sqrt{s_0 - s}}.$$

The six free parameters α_V, κ, m_ω, m_ρ, B_0 and B_1 are determined by the fit to the $\pi^+\pi^-$ data restricted to the region up to 1 GeV to stay below the threshold of significant inelastic channels. The width of the ω resonance is fixed to its PDG value of 8.49 MeV [6], and $\sqrt{s_0} = 1.05$ GeV. The results of the fit are given in Table 1. To derive an estimate for the model uncertainty, we independently vary $\sqrt{s_0}$ to 1.3 GeV and remove the linear term $B_1\omega(s)$ from Eq. (5) since the resulting value of B_1 from the nominal fit is consistent with zero.

The fit is performed using as test statistic a diagonal χ^2 function that accounts for the statistical and systematic uncertainties of the experimental measurements.[7] The same uncertainty rescaling in case of local discrepancies among datasets as for the HVPTools based combination is applied. Correlations are ignored in the test statistic, but accounted for in the uncertainty propagation through a series of pseudo-experiments for each of which the full fit procedure is repeated. This is a conservative procedure, as exploiting correlations in the test statistic would improve the precision of the fit. Currently, the most precise measurements are dominated by systematic uncertainties, whose size and mass dependence as well as correlation among each other and among data points rely on estimates with somewhat limited precision, as discussed in Sect. 2. Since there are also clear

---

[7] For the fit we use the original data provided by each experiment instead of the HVPTools combination.
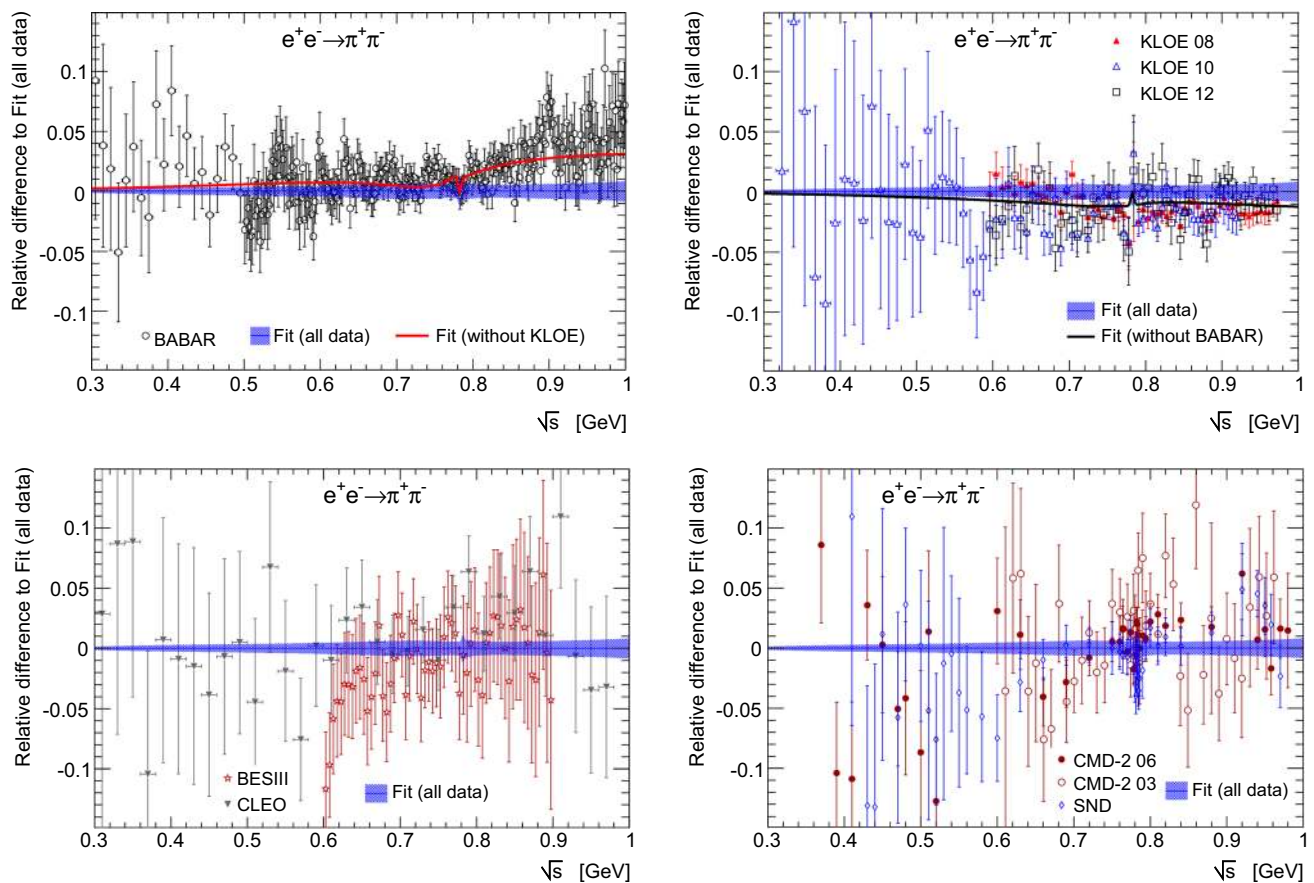
Fig. 4 Same as Fig. 2 except that the comparison is made with respect to the fit instead of the combination. The black and red curves show the results of two alternative fits where the data from KLOE and BABAR, respectively, were excluded

indications of a significant underestimate of the size of uncertainties in the discrepant dataset(s), we prefer not to exploit this information in the constrained fit. Pseudo-experiments are also used to assess the goodness-of-fit on the data, which yields a p-value of 0.27.[8] We have checked the reliability of this procedure by generating a set of pseudo-experiments and evaluating the p-value for each of them. The expected distribution of p-values reconstructed this way is indeed uniform between 0 and 1.

A graphical comparison of the fit result with the data is shown in Fig. 4. In the energy range between 0.3 and 0.6 GeV, the result of the fit yields for $a_\mu^{\mathrm{had,LO}}[\pi\pi]$ a contribution of $109.8 \pm 0.4 \pm 0.4$, where the first error is experimental and the second the model uncertainty. The latter is obtained by adding linearly the absolute values of following two variations: the $\sqrt{s_0}$ variation of -0.13 ± 0.10 and the difference of without and with the $B_1\omega(s)$ term of 0.24 ± 0.14, where the uncertainty of each variation accounts for the correlation

between the integral results. The corresponding result based on data integration is 109.6 ± 1.0. Taking into account the correlation of 72% between the experimental uncertainties, the difference between the two evaluations amounts to 0.2 ± 0.9. Similarly, for $\Delta\alpha_{\mathrm{had}}(m_Z^2)$ the difference is 0.020 ± 0.028. The fit therefore gives compatible but more precise results than the direct data integration.

Other studies using constraints from unitarity and analyticity with the aim to improve the precision of the $\pi^+\pi^-$ HVP contribution to the muon $g - 2$ exist in the literature.[9] The treatment followed in Ref. [38] is similar to ours with, however, a more elaborate theoretical analysis. Differences are also present in the treatment of experimental data, Ref. [38] using a χ^2 computed globally, including correlations across all the experimental data points and bins in the full mass range of interest. However, in order to avoid too low p-values, some bins of the KLOE measurements were removed in that study and energy rescaling parameters were introduced to fit each measured energy spectrum. A different approach is followed in Ref. [39,40] where the low-mass contribution was

---

[8] The p-values for each individual dataset read 0.042 (BABAR), 0.097 (KLOE), 0.449 (CMD), 0.675 (TOF), 0.718 (DM1), 0.756 (CMD-2), 0.796 (SND), and 0.984 (CLEO). The p-values for both OLYA and BESIII are close to 1.

[9] In Ref. [37] an analyticity-based phenomenological fit has been used for the $\pi^+\pi^-\pi^0$ channel.

obtained from input data at a fixed mass, followed by a simple average used to combine inputs in the $\sqrt{s}$ range between 0.65 and 0.71 GeV (and then to combine values from different experiments). Instead of a direct evaluation of the correlations from the published information, they were assumed to be the same between all the combination inputs and an attempt was made to evaluate them based on the resulting χ^2 value. It is possible to directly compare the results for the mass region between threshold and 0.63 GeV. In the present analysis a value of $133.2 \pm 0.5 \pm 0.4$ is found, which agrees with the other results, $132.8 \pm 0.4 \pm 1.0$ [38] and 132.9 ± 0.8 [39,40].

It is also interesting to compare the results given in Table 1 with other analyses. The value obtained for κ corresponds to a branching fraction of ω into $\pi^+\pi^-$ of $(2.09 \pm 0.09) \cdot 10^{-2}$, in agreement with the result extracted from the fit of Ref. [38], $(1.95 \pm 0.08) \cdot 10^{-2}$. Both values disagree with the PDG average [6], $(1.51 \pm 0.12) \cdot 10^{-2}$, dominated by the result of Ref. [33] which uses fits to essentially the same data. The fitted ω mass is found to be lower than the PDG average [6] obtained from 3π decays by $(0.65 \pm 0.12 \pm 0.12_{\text{PDG}})$ MeV, in agreement with previous fits of the $\rho - \omega$ interference in the 2π spectrum (see for instance Refs. [21,38]).

The $\pi^+\pi^-$ contribution

The evaluation of the complete $a_\mu^{\text{had,LO}}[\pi\pi]$ integral for the $\pi^+\pi^-$ contribution from threshold to 1.8 GeV, using the fit up to 0.6 GeV and the HVPTools data combination above, gives 507.0 ± 1.9. The choice of the ranges is justified by the good agreement between fit and combined data integration in the 0.6–1.0 GeV region with, however, no advantage in precision for the fit. The correlation among the two contributions is found to be 62% using pseudo-experiments.

Removing BABAR or KLOE from the dataset gives 505.1 ± 2.1 and 510.6 ± 2.2, respectively, with an absolute difference of 5.5 that is significantly larger than the individual uncertainties. Figure 5 shows a comparison among the most precise $a_\mu^{\text{had,LO}}[\pi\pi]$ evaluations in the interval 0.6–0.9 GeV. The results of all other experiments fall in-between the BABAR and KLOE results, with insufficient precision to resolve the discrepancy.

Figure 6 compares the HVPTools combination and the fits without using the BABAR and KLOE data, respectively, with the fit result for the full dataset. In light of this discrepancy, which is not fully captured by the local uncertainty rescaling procedure, we add as additional systematic uncertainty half of the full difference between the complete integrals without BABAR and KLOE, respectively, and we place the central value of the $a_\mu^{\text{had,LO}}[\pi\pi]$ contribution half-way between the two results. To avoid double counting, the local uncertainty rescaling between BABAR and KLOE is not applied, but that between these and the other $\pi^+\pi^-$ datasets
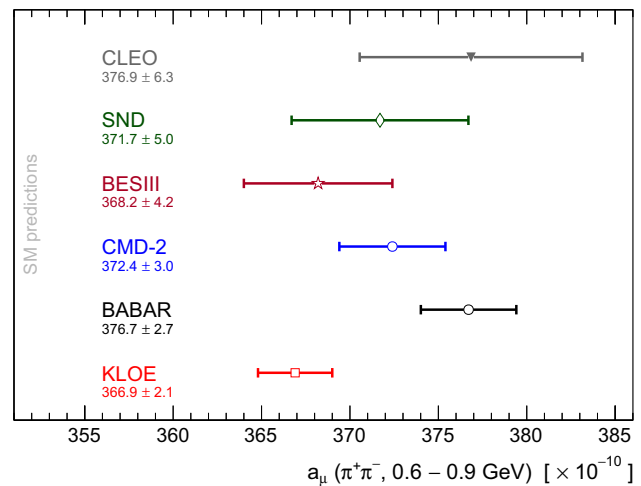

Fig. 5 Comparison of results for $a_\mu^{\text{had,LO}}[\pi\pi]$, evaluated between 0.6 GeV and 0.9 GeV for the various experiments. In case of CMD-2 all available measurements have been combined using HVPTools. For KLOE the result from the public combination [27] is displayed
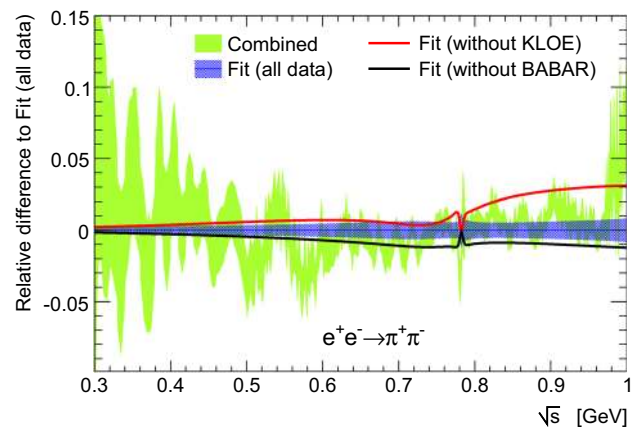

Fig. 6 The HVPTools combination (green band) relative to the result of the fit to all individual $\pi^+\pi^-$ data (blue band) versus centre-of-mass energy. The black and red curves show the results of two alternative fits where the data from KLOE and BABAR, respectively, were excluded

is kept. This procedure results in a total $\pi^+\pi^-$ contribution of $a_\mu^{\text{had,LO}}[\pi\pi] = 507.9 \pm 0.8 \pm 3.2$, where the first uncertainty is statistical and the second systematic (dominated by the new uncertainty of 2.8).

3.2 The K^+K^- channel

Tensions among datasets are also present in the K^+K^- channel (see top panel of Fig. 7 for a display of the available measurements). A discrepancy between BABAR and SND was observed for masses between 1.05 and 1.4 GeV, which has been resolved with the most recent SND result [41] so that older SND data are discarded.

Concerns also arise regarding data on the $\phi(1020)$ resonance. Previously, a 5.1% difference between CMD-2 at

VEPP-2M and BABAR was observed, with the CMD-2 data being lower. New results from CMD-3 at VEPP-2000 [42] exhibit the opposite effect: they are 5.5% higher than BABAR (cf. middle panel in Fig. 7). The discrepancy of almost 11% between the CMD-2 and CMD-3 datasets, which largely exceeds the quoted systematic uncertainty of 2.2%, of which only 1.2% accounts for uncertainties in the detection efficiency, is claimed to originate from a better understanding of the detection efficiency of low-energy kaons in the CMD-3 data.[10] Given the yet unresolved situation, we keep both CMD-2 and CMD-3 datasets, which due to the uncertainty rescaling procedure in presence of discrepancies leads to a deterioration of the precision by about a factor of two of the combined data (cf. bottom panel of Fig. 7).[11]

3.3 Other channels

Recent measurements have been included in the data combinations: $\pi^0\gamma$ from SND [12], $\pi^+\pi^-2\pi^0$ from BABAR [8], $\pi^+\pi^-3\pi^0$ from BABAR [13], $\eta\pi^+\pi^-$ from BABAR [11], $\eta\pi^+\pi^-\pi^0$ from CMD-3 [7] and SND [15], $\phi\eta$ from CMD-3 [16], and $K_S K_L \pi^0$ from SND [9]. The $\pi^0\gamma$ and $\pi^+\pi^-\pi^0$ contributions include small additions of 0.12 ± 0.01 and 0.01 ± 0.00, respectively, to cover the threshold region up to the lowest-energy data measurements [43,44].

Only very few final states remain to be estimated using isospin symmetry. Already in 2017, a significant step was achieved with the BABAR measurements of all the final states contributing to the $K\overline{K}\pi$ and $K\overline{K}\pi\pi$ channels, so that previous isospin-based estimates became obsolete. Now the only significant (albeit small) contribution obtained with the use of isospin constraints is that for the $\pi^+\pi^-4\pi^0$ channel. The part excluding $\eta3\pi$, which is obtained from measured processes and reevaluated in this analysis, amounts to a fraction of the total dispersion integral of only 0.016% with an assigned systematic uncertainty of 100%. One could also question the completeness of the set of exclusive processes considered below 1.8 GeV, including up to 6-pion and $K\overline{K}+3$ pions. A recent measurement of the $3\pi^+3\pi^-\pi^0$ cross section by CMD-3 [14] allows one to estimate a very small total 7-pion contribution, included in this analysis, of only 0.002%. Although such high-multiplicity channels appear to be con-

---

[10] In comparison with the CMD-2/3 and SND measurements, the ISR method of BABAR benefits from higher-momentum kaons with better detection efficiency owing to the boost of the final state.

[11] We have verified that the local χ^2 rescaling procedure covers the global discrepancy among the CMD-2 and CMD-3 data by removing alternatively one or the other dataset from the K^+K^- combination. The difference of 0.45 resulting between the two a_μ values is covered by the uncertainty rescaling (a similar conclusion is reached for $\Delta\alpha_{\text{had}}(m_Z^2)$). There is therefore no need to introduce an additional global systematic uncertainty as for the $\pi^+\pi^-$ case.
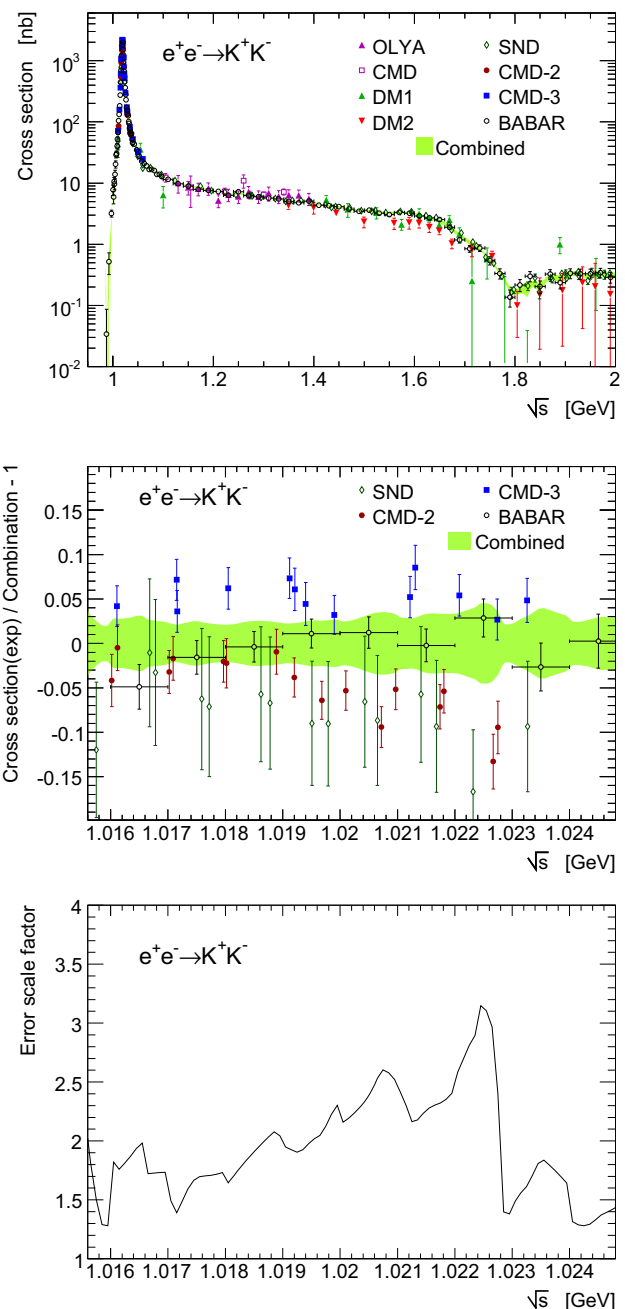
Fig. 7 Top panel: bare cross sections for $e^+e^- \rightarrow K^+K^-$. See text for a description of the data used. Middle: comparison between individual $e^+e^- \rightarrow K^+K^-$ cross-section measurements from BABAR [45], CMD-2 [46], CMD-3 [42] and SND [41], and the HVPTools combination. Bottom: local scale factor versus centre-of-mass energy applied to the combined K^+K^- cross-section uncertainty to account for inconsistency in the individual measurements

tributing negligibly below 1.8 GeV their importance is likely to increase above.

All other contributions are identical to the ones described in our previous analysis [1], except for (i) a reevaluation of the contribution from ω decay modes not reconstructed in

other exclusive channels, and (ii) a better estimate of the $K\overline{K}\pi^+\pi^-\pi^0$ contribution, excluding $\phi\eta$ which is dominated by the $K\overline{K}\omega$ final state [47].

4 Compilation and results

A compilation of the various contributions to $a_\mu^{\text{had,LO}}$ and to $\Delta\alpha_{\text{had}}(m_Z^2)$, as well as the total results are given in Table 2. The experimental uncertainties are separated into statistical, channel-specific systematic, and common systematic contributions that are correlated with at least one other channel.

The contributions from the J/ψ and $\psi(2S)$ resonances in Table 2 are obtained by numerically integrating the corresponding undressed[12] Breit–Wigner lineshapes. The uncertainties in the integrals are dominated by the knowledge of the corresponding electronic width $\Gamma_{R\rightarrow ee}$ for which we use the values 5.53 ± 0.10 keV for $R = J/\psi$ and 2.34 ± 0.04 keV for $R = \psi(2S)$ [6].

Sufficiently far from the quark thresholds we use four-loop [20] perturbative QCD, including $\mathcal{O}(\alpha_s^2)$ quark mass corrections [48], to compute the inclusive hadronic cross section. Nonperturbative contributions at 1.8 GeV were determined from data [49] and found to be small. The uncertainties of the R_{QCD} contributions given in Table 2 are obtained from the quadratic sum of the uncertainty in α_S (we use $\alpha_S(m_Z^2) = 0.1193 \pm 0.0028$ from the fit to Z precision data [50]), the truncation of the perturbative series (we use the full four-loop contribution as systematic uncertainty), the difference between fixed-order perturbation theory (FOPT) and, so-called, contour-improved perturbation theory (CIPT) [51], as well as quark mass uncertainties (we use the values and uncertainties from Ref. [6]). The former three uncertainties are taken to be fully correlated between the various energy regions (see Table 2), whereas the (smaller) quark-mass uncertainties are taken to be uncorrelated.

To examine the transition region between the sum of exclusive measurements and QCD we have computed $a_\mu^{\text{had,LO}}$ and $\Delta\alpha_{\text{had}}(m_Z^2)$ in the narrow energy interval 1.8–2.0 GeV. For the former quantity we find 7.65 ± 0.31 and 8.30 ± 0.09 for data and QCD, respectively. The full difference of 0.65 ($0.28 \cdot 10^{-4}$ in the case of $\Delta\alpha_{\text{had}}(m_Z^2)$) is assigned as additional systematic uncertainty, labelled by "dual" subscripts in Table 2. It accounts for possible low-mass quark-hadron duality violation effects in the perturbative QCD approxima-

tion that we use for this interval to avoid systematic effects due to unmeasured high-multiplicity channels.

Figure 8 shows the total hadronic e^+e^- annihilation rate R versus centre-of-mass energy as obtained from the sum of exclusive data below 2 GeV and from inclusive data between 1.8 and 5 GeV.[13] Also indicated are the perturbative QCD prediction above 1.5 GeV and the analytical narrow J/ψ and $\psi(2S)$ resonances.

Muon magnetic anomaly Adding all lowest-order hadronic contributions together gives

$$a_\mu^{\text{had,LO}} = 694.0 \pm 4.0, \tag{6}$$

which is dominated by experimental systematic uncertainties (cf. Table 2 for a separation of the total uncertainty into its components), with an uncertainty of 2.8 originating from the BABAR versus KLOE discrepancy in the $\pi^+\pi^-$ channel. The new result is 0.9 units larger than our previous evaluation [1], 693.1 ± 3.4, mostly because we symmetrised the new BABAR/KLOE systematic uncertainty. The total uncertainty is increased by 18%. The result without the additional BABAR/KLOE systematic uncertainty is 693.1 ± 3.2.

Adding to (6) the contributions from higher order hadronic loops, -9.87 ± 0.09 (NLO) and 1.24 ± 0.01 (NNLO) [58], hadronic light-by-light scattering, 10.5 ± 2.6 [59], as well as QED, $11,658,471.895 \pm 0.008$ [60] (see also [61] and references therein), and electroweak effects, 15.36 ± 0.10 [62–65],[14] we obtain the complete SM prediction

$$a_\mu^{\text{SM}} = 11,659,183.1 \pm 4.0 \pm 2.6 \pm 0.1\ (4.8_{\text{tot}}), \tag{7}$$

where the uncertainties account for lowest and higher order hadronic, and other contributions, respectively. The result (7) deviates from the experimental value, $a_\mu^{\text{exp}} = 11\,659\,209.1 \pm 5.4 \pm 3.3$ [61,68], by 26.0 ± 7.9 (3.3σ).

A compilation of recent SM predictions for a_μ compared with the experimental result is given in Fig. 9.

Running electromagnetic coupling at m_Z^2 The sum of all quark-flavour terms from Table 2 gives for the hadronic contribution to the running of $\alpha(m_Z^2)$

$$\Delta\alpha_{\text{had}}(m_Z^2) = (275.3 \pm 1.0) \cdot 10^{-4}, \tag{8}$$

the uncertainty of which is dominated by data systematic effects ($0.7 \cdot 10^{-4}$) and the uncertainty in the QCD prediction ($0.6 \cdot 10^{-4}$). The use of the same inputs with different

---

[12] The undressing uses the BABAR programme AFKVAC, correcting for both leptonic and hadronic VP effects. The hadronic part is obtained from a numerical integration over cross section data for the continuum, supplemented by analytical expressions for the contributions of narrow resonances including both their real and imaginary components. The resulting correction factors reduce the J/ψ and $\psi(2S)$ contributions to $a_\mu^{\text{had,LO}}$ by about 4% and are known to a precision of better than 10^{-3}.

[13] We have verified that the integration of the finely binned R distribution shown in Fig. 8, together with its covariance matrix, accurately reproduces the $a_\mu^{\text{had,LO}}$ and $\Delta\alpha_{\text{had}}(m_Z^2)$ results obtained by summing the exclusive modes below 1.8 GeV in Table 2.

[14] When adjusting [66] the new full 2-loop calculation in Ref. [67] to physical quark masses, it reproduces the value obtained in [62].

Table 2 Compilation of the contributions to $a_\mu^{\mathrm{had,LO}}$ and $\Delta\alpha_{\mathrm{had}}(m_Z^2)$ as obtained from HVPTools, and the phenomenological fit for the $\pi^+\pi^-$ contribution below 0.6 GeV. Where three (or more) uncertainties are given, the first is statistical, the second channel-specific systematic, and the third common systematic, which is correlated with at least one other channel. For the contributions computed from QCD, only total uncertainties are given, which include effects from the α_s uncertainty, the truncation of the perturbative series at four loops, the FOPT vs. CIPT ambiguity, and quark mass uncertainties. Except for the latter uncertainty, all other uncertainties are taken to be fully correlated among the various energy regions where QCD is used. The additional uncertainty dubbed "dual" estimates possible quark-hadron duality violating effects in the QCD estimate between 1.8 and 2.0 GeV. The uncertainties in the Breit–Wigner integrals of the narrow resonances J/ψ and $\psi(2S)$ are dominated by the respective electronic width measurements [6]. The uncertainties in the sums (last line) are obtained by quadratically adding all statistical and channel-specific systematic uncertainties, and by linearly adding correlated inter-channel systematic uncertainties

Channel	$a_\mu^{\mathrm{had,LO}}$ $[10^{-10}]$	$\Delta\alpha_{\mathrm{had}}(m_Z^2)$ $[10^{-4}]$
$\pi^0\gamma$	$4.41 \pm 0.06 \pm 0.04 \pm 0.07$	$0.35 \pm 0.00 \pm 0.00 \pm 0.01$
$\eta\gamma$	$0.65 \pm 0.02 \pm 0.01 \pm 0.01$	$0.08 \pm 0.00 \pm 0.00 \pm 0.00$
$\pi^+\pi^-$	$507.85 \pm 0.83 \pm 3.23 \pm 0.55$	$34.50 \pm 0.06 \pm 0.20 \pm 0.04$
$\pi^+\pi^-\pi^0$	$46.21 \pm 0.40 \pm 1.10 \pm 0.86$	$4.60 \pm 0.04 \pm 0.11 \pm 0.08$
$2\pi^+2\pi^-$	$13.68 \pm 0.03 \pm 0.27 \pm 0.14$	$3.58 \pm 0.01 \pm 0.07 \pm 0.03$
$\pi^+\pi^-2\pi^0$	$18.03 \pm 0.06 \pm 0.48 \pm 0.26$	$4.45 \pm 0.02 \pm 0.12 \pm 0.07$
$2\pi^+2\pi^-\pi^0$ (η excl.)	$0.69 \pm 0.04 \pm 0.06 \pm 0.03$	$0.21 \pm 0.01 \pm 0.02 \pm 0.01$
$\pi^+\pi^-3\pi^0$ (η excl.)	$0.49 \pm 0.03 \pm 0.09 \pm 0.00$	$0.15 \pm 0.01 \pm 0.03 \pm 0.00$
$3\pi^+3\pi^-$	$0.11 \pm 0.00 \pm 0.01 \pm 0.00$	$0.04 \pm 0.00 \pm 0.00 \pm 0.00$
$2\pi^+2\pi^-2\pi^0$ (η excl.)	$0.71 \pm 0.06 \pm 0.07 \pm 0.14$	$0.25 \pm 0.02 \pm 0.02 \pm 0.05$
$\pi^+\pi^-4\pi^0$ (η excl., isospin)	$0.08 \pm 0.01 \pm 0.08 \pm 0.00$	$0.03 \pm 0.00 \pm 0.03 \pm 0.00$
$\eta\pi^+\pi^-$	$1.19 \pm 0.02 \pm 0.04 \pm 0.02$	$0.35 \pm 0.01 \pm 0.01 \pm 0.01$
$\eta\omega$	$0.35 \pm 0.01 \pm 0.02 \pm 0.01$	$0.11 \pm 0.00 \pm 0.01 \pm 0.00$
$\eta\pi^+\pi^-\pi^0$(non-ω,ϕ)	$0.34 \pm 0.03 \pm 0.03 \pm 0.04$	$0.12 \pm 0.01 \pm 0.01 \pm 0.01$
$\eta2\pi^+2\pi^-$	$0.02 \pm 0.01 \pm 0.00 \pm 0.00$	$0.01 \pm 0.00 \pm 0.00 \pm 0.00$
$\omega\eta\pi^0$	$0.06 \pm 0.01 \pm 0.01 \pm 0.00$	$0.02 \pm 0.00 \pm 0.00 \pm 0.00$
$\omega\pi^0$ ($\omega \to \pi^0\gamma$)	$0.94 \pm 0.01 \pm 0.03 \pm 0.00$	$0.20 \pm 0.00 \pm 0.01 \pm 0.00$
$\omega2\pi$ ($\omega \to \pi^0\gamma$)	$0.07 \pm 0.00 \pm 0.00 \pm 0.00$	$0.02 \pm 0.00 \pm 0.00 \pm 0.00$
ω (non-$3\pi, \pi\gamma, \eta\gamma$)	$0.04 \pm 0.00 \pm 0.00 \pm 0.00$	$0.00 \pm 0.00 \pm 0.00 \pm 0.00$
K^+K^-	$23.08 \pm 0.20 \pm 0.33 \pm 0.21$	$3.35 \pm 0.03 \pm 0.05 \pm 0.03$
$K_S K_L$	$12.82 \pm 0.06 \pm 0.18 \pm 0.15$	$1.74 \pm 0.01 \pm 0.03 \pm 0.02$
ϕ (non-$K\overline{K}, 3\pi, \pi\gamma, \eta\gamma$)	$0.05 \pm 0.00 \pm 0.00 \pm 0.00$	$0.01 \pm 0.00 \pm 0.00 \pm 0.00$
$K\overline{K}\pi$	$2.45 \pm 0.05 \pm 0.10 \pm 0.06$	$0.78 \pm 0.02 \pm 0.03 \pm 0.02$
$K\overline{K}2\pi$	$0.85 \pm 0.02 \pm 0.05 \pm 0.01$	$0.30 \pm 0.01 \pm 0.02 \pm 0.00$
$K\overline{K}\omega$	$0.00 \pm 0.00 \pm 0.00 \pm 0.00$	$0.00 \pm 0.00 \pm 0.00 \pm 0.00$
$\eta\phi$	$0.33 \pm 0.01 \pm 0.01 \pm 0.00$	$0.11 \pm 0.00 \pm 0.00 \pm 0.00$
$\eta K\overline{K}$ (non-ϕ)	$0.01 \pm 0.01 \pm 0.01 \pm 0.00$	$0.00 \pm 0.00 \pm 0.01 \pm 0.00$
$\omega3\pi$ ($\omega \to \pi^0\gamma$)	$0.06 \pm 0.01 \pm 0.01 \pm 0.01$	$0.02 \pm 0.00 \pm 0.00 \pm 0.00$
7π ($3\pi^+3\pi^-\pi^0$ + estimate)	$0.02 \pm 0.00 \pm 0.01 \pm 0.00$	$0.01 \pm 0.00 \pm 0.00 \pm 0.00$
J/ψ (BW integral)	6.20 ± 0.11	7.00 ± 0.13
$\psi(2S)$ (BW integral)	1.56 ± 0.05	2.48 ± 0.08
R data $[3.7 - 5.0]$ GeV	$7.29 \pm 0.05 \pm 0.30 \pm 0.00$	$15.79 \pm 0.12 \pm 0.66 \pm 0.00$
R_{QCD} $[1.8 - 3.7$ GeV$]_{uds}$	$33.45 \pm 0.28 \pm 0.65_{\mathrm{dual}}$	$24.27 \pm 0.18 \pm 0.28_{\mathrm{dual}}$
R_{QCD} $[5.0 - 9.3$ GeV$]_{udsc}$	6.86 ± 0.04	34.89 ± 0.18
R_{QCD} $[9.3 - 12.0$ GeV$]_{udscb}$	1.20 ± 0.01	15.53 ± 0.04
R_{QCD} $[12.0 - 40.0$ GeV$]_{udscb}$	1.64 ± 0.00	77.94 ± 0.13
R_{QCD} $[> 40.0$ GeV$]_{udscb}$	0.16 ± 0.00	42.70 ± 0.05
R_{QCD} $[> 40.0$ GeV$]_t$	0.00 ± 0.00	-0.72 ± 0.01
Sum	$694.0 \pm 1.0 \pm 3.5 \pm 1.6 \pm 0.1_\psi \pm 0.7_{\mathrm{QCD}}$	$275.29 \pm 0.15 \pm 0.72 \pm 0.23 \pm 0.15_\psi \pm 0.55_{\mathrm{QCD}}$

Fig. 8 The total hadronic e^+e^- annihilation rate R as a function of centre-of-mass energy. Inclusive measurements from BES [52–55] and KEDR [56,57] are shown as data points, while the sum of exclusive channels from this analysis is given by the narrow blue bands. Also shown for the purpose of illustration is the prediction from massless perturbative QCD (solid red line)
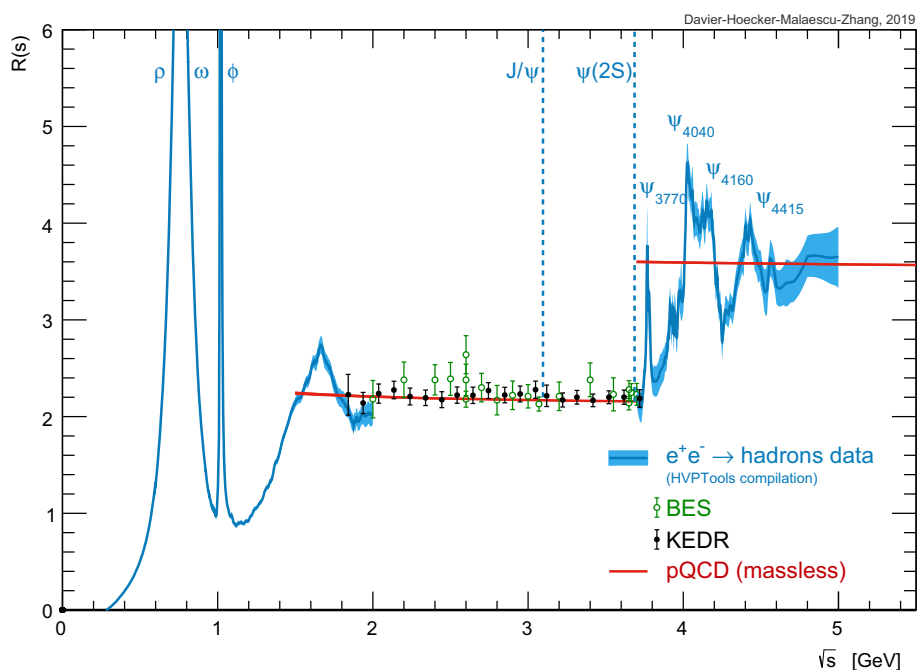
integration kernels in the calculations induces a correlation of + 44% between the $a_\mu^{\mathrm{had,LO}}$ and $\Delta\alpha_{\mathrm{had}}(m_Z^2)$ uncertainties. The result without the new BABAR/KLOE systematic uncertainty is 275.2 ± 0.9.

Adding to (8) the four-loop leptonic contribution, $\Delta\alpha_{\mathrm{lep}}(m_Z^2) = (314.979 \pm 0.002) \cdot 10^{-4}$ [70], one finds

$$\alpha^{-1}(m_Z^2) = 128.947 \pm 0.013. \tag{9}$$

The current uncertainty on $\alpha(m_Z^2)$ is sub-dominant in the SM prediction of the W-boson mass (the dominant uncertainties are due to the top mass and of theoretical origin), but dominates the prediction of $\sin^2\theta_{\mathrm{eff}}^\ell$, which, however, is about twice more accurate than the combination of all present measurements [50].

5 Conclusions and perspectives

Using newest available $e^+e^- \rightarrow$ hadrons cross-section data we have reevaluated the lowest-order hadronic vacuum polarisation contribution to the Standard Model prediction of the anomalous magnetic moment of the muon, and the hadronic contribution to the running electromagnetic coupling strength at the Z-boson mass. For the former quantity we find $a_\mu^{\mathrm{had,LO}} = (694.0 \pm 4.0) \cdot 10^{-10}$. In spite of new data and the use of a more precise fit to evaluate the threshold region up to 0.6 GeV, the uncertainty on this contribution has increased to 0.6% since our last evaluation [1], due to the addition of a new systematic uncertainty to account for a global discrepancy between $\pi^+\pi^-$ data from BABAR and
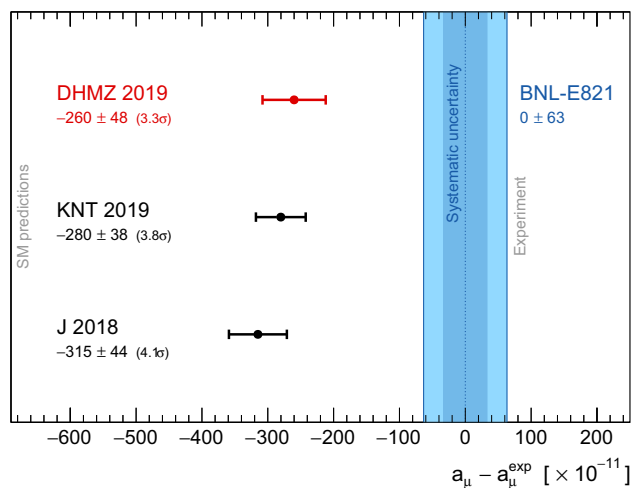
Fig. 9 Compilation of recent data-driven results for a_μ^{SM} (in units of 10^{-10}), subtracted by the central value of the experimental average [61, 68]. The blue vertical band indicates the experimental uncertainty, with the darker inlet representing the experimental systematic uncertainty. The representative SM predictions are taken from KNT 2019 [44], J 2018 [69], and this work (DHMZ 2019)

KLOE. Resolving this discrepancy would allow to reduce the $a_\mu^{\mathrm{had,LO}}$ uncertainty by 20%.[15]

The discrepancy between measurement and complete Standard Model prediction remains at a non-conclusive 3.3σ level. The new Fermilab $g-2$ experiment currently in operation [71] aims at up to four times better ultimate precision and has the potential to clarify the situation.

---

[15] The contribution of the $\pi^+\pi^-$ channel to the total $a_\mu^{\mathrm{had,LO}}$ uncertainty-squared is 71%.

To match the precision of the new experiment further progress is needed to reduce the uncertainty on $a_\mu^{\text{had,LO}}$ from dispersion relations. New analyses of the dominant $\pi^+\pi^-$ channel are underway at the BABAR, CMD-3 and SND experiments for which a systematic uncertainty below 0.5% may be reachable. It is also important to improve the precision of the $\pi^+\pi^-\pi^0$ and K^+K^- channels. The new Belle-2 experiment at the KEK Super-B factory will also contribute to measuring hadronic cross sections via the ISR method once the detector performance is fully understood and sufficient statistics has been accumulated.

Independently of the data-driven approach, lattice QCD calculations of $a_\mu^{\text{had,LO}}$ are also progressing albeit not yet reaching competitive precision [72–79].

The determination of $a_\mu^{\text{had,LO}}$ is closing in on the estimated uncertainty of the hadronic light-by-light scattering contribution $a_\mu^{\text{had,LBL}}$ of $2.6 \cdot 10^{-10}$, which appears irreducible at present. Here only phenomenological models have been used so far and lattice QCD calculations could have a strong impact [80], as well as a new promising dispersive approach [81].

Data Availability Statement This manuscript has no associated data or the data will not be deposited. [Authors' comment: The relevant numerical results of the study are already provided in the paper.]

References

1. M. Davier, A. Hoecker, B. Malaescu, Z. Zhang, Eur. Phys. J. C **77**, 827 (2017). arXiv:1706.09436
2. M. Davier, A. Hoecker, B. Malaescu, C.Z. Yuan, Z. Zhang, Eur. Phys. J. C **66**, 1 (2010). arXiv:0908.4300
3. ATLAS Collaboration, Eur. Phys. J. C **75**, 17 (2015). arXiv:1406.0076
4. ATLAS Collaboration, JHEP **09**, 020 (2017). arXiv:1706.03192
5. ATLAS Collaboration, JHEP **05**, 195 (2018). arXiv:1711.02692
6. Particle Data Group, Phys. Rev. D **98**, 030001 (2018). 2019 update. http://pdglive.lbl.gov
7. CMD-3 Collaboration, Phys. Lett. B **773**, 150 (2017). arXiv:1706.06267
8. BABAR Collaboration, Phys. Rev. D **96**, 092009 (2017). arXiv:1709.01171
9. M.N. Achasov et al., Phys. Rev. D **97**, 032011 (2018). arXiv:1711.07143
10. T. Xiao, S. Dobbs, A. Tomaradze, K.K. Seth, G. Bonvicini, Phys. Rev. D **97**, 032012 (2018). arXiv:1712.04530
11. BABAR Collaboration, Phys. Rev. D **97**, 052007 (2018). arXiv:1801.02960
12. M.N. Achasov et al., Phys. Rev. D **98**, 112001 (2018). arXiv:1809.07631
13. BABAR Collaboration, Phys. Rev. D **98**, 112015 (2018). arXiv:1810.11962
14. CMD-3 Collaboration, Phys. Lett. B **792**, 419 (2019). arXiv:1902.06449
15. M.N. Achasov et al., Phys. Rev. D **99**, 112004 (2019). arXiv:1903.09307
16. V.L. Ivanov et al., Phys. Lett. B **798**, 134946 (2019). arXiv:1906.08006
17. M. Davier, A. Hoecker, B. Malaescu, Z. Zhang, Eur. Phys. J. C **71**, 1515 (2011). arXiv:1010.4180
18. M. Davier, S. Eidelman, A. Hoecker, Z. Zhang, Eur. Phys. J. C **27**, 497 (2003). arXiv:hep-ph/0208177
19. M. Davier, S. Eidelman, A. Hoecker, Z. Zhang, Eur. Phys. J. C **31**, 503 (2003). arXiv:hep-ph/0308213
20. P.A. Baikov, K.G. Chetyrkin, J.H. Kühn, Phys. Rev. Lett. **101**, 012002 (2008). arXiv:0801.1821
21. BABAR Collaboration, Phys. Rev. D **8**, 032013 (2012). arXiv:1205.2228
22. BABAR Collaboration, Phys. Rev. Lett. **103**, 231801 (2009). arXiv:0908.3589
23. KLOE Collaboration, Phys. Lett. B **670**, 285 (2009). arXiv:0809.3950
24. KLOE Collaboration, Phys. Lett. B **700**, 102 (2011). arXiv:1006.5313
25. KLOE Collaboration, Phys. Lett. B **720**, 336 (2013). arXiv:1212.4524
26. BESIII Collaboration, Phys. Lett. B **753**, 629 (2015). arXiv:1507.08188
27. KLOE-2 Collaboration, JHEP **03**, 173 (2018). arXiv:1711.03085
28. CMD-2 Collaboration, Phys. Lett. B **578**, 285 (2004). arXiv:hep-ex/0308008
29. CMD-2 Collaboration, JETP Lett. **82**, 743 (2005). arXiv:hep-ex/0603021
30. CMD-2 Collaboration, JETP Lett. **84**, 413 (2006). arXiv:hep-ex/0610016
31. CMD-2 Collaboration, Phys. Lett. B **648**, 28 (2007). arXiv:hep-ex/0610021
32. SND Collaboration, JETP Lett. **103**, 380 (2006). arXiv:hep-ex/0605013
33. C. Hanhart, S. Holz, B. Kubis, A. Kupść, A. Wirzba, C.W. Xiao, Eur. Phys. J. C **77**, 98 (2017). Erratum: [Eur. Phys. J. C **78**, 450 (2018)]. arXiv:1611.09359
34. J.F. De Troconiz, F.J. Yndurain, Phys. Rev. D **65**, 093001 (2002). arXiv:hep-ph/0106025
35. J.F. de Troconiz, F.J. Yndurain, Phys. Rev. D **71**, 073008 (2005). arXiv:hep-ph/0402285
36. R. Garcia-Martin, R. Kaminski, J.R. Pelaez, J. Ruiz de Elvira, F.J. Yndurain, Phys. Rev. D **83**, 074004 (2011). arXiv:1102.2183
37. M. Hoferichter, B.L. Hoid, B. Kubis, JHEP **08**, 137 (2019). arXiv:1907.01556
38. G. Colangelo, M. Hoferichter, P. Stoffer, JHEP **02**, 006 (2019). arXiv:1810.00007
39. B. Ananthanarayan, I. Caprini, D. Das, Phys. Rev. D **98**, 114015 (2018). arXiv:1810.09265
40. B. Ananthanarayan, I. Caprini, D. Das, Rom. J. Phys. **64**, 401 (2019). arXiv:1907.01767
41. SND Collaboration, Phys. Rev. D **94**, 112006 (2016). arXiv:1608.08757

42. E.A. Kozyrev et al., Phys. Lett. B **779**, 64 (2018). arXiv:1710.02989
43. K. Hagiwara, A.D. Martin, D. Nomura, T. Teubner, Phys. Rev. D **69**, 093003 (2004). arXiv:hep-ph/0312250
44. A. Keshavarzi, D. Nomura, T. Teubner, Phys. Rev. D **101**, 014029 (2020). arXiv:1911.00367
45. BABAR Collaboration, Phys. Rev. D **88**, 032013 (2013). arXiv:1306.3600
46. CMD-2 Collaboration, Phys. Lett. B **669**, 217 (2008). arXiv:0804.0178
47. BABAR Collaboration, Phys. Rev. D **76**, 092005 (2007). Erratum: Phys. Rev. D **77**, 119902 (2008). arXiv:0708.2461
48. K.G. Chetyrkin, J.H. Kühn, M. Steinhauser, Nucl. Phys. B **482**, 213 (1996). arXiv:hep-ph/9606230
49. M. Davier, A. Hoecker, Phys. Lett. B **419**, 419 (1998). arXiv:hep-ph/9801361
50. Gfitter Group, Eur. Phys. J. C **74**, 3046 (2014). arXiv:1407.3792
51. F. Le Diberder, A. Pich, Phys. Lett. B **286**, 147 (1992)
52. BES Collaboration, Phys. Rev. Lett. **84**, 594 (2000). arXiv:hep-ex/9908046
53. BES Collaboration, Phys. Rev. Lett. **88**, 101802 (2002). arXiv:hep-ex/0102003
54. BES Collaboration, Phys. Lett. B **641**, 145 (2006). arXiv:hep-ex/0605105
55. BES Collaboration, Phys. Lett. B **677**, 239 (2009). arXiv:0903.0900
56. KEDR Collaboration, Phys. Lett. B **753**, 533 (2016). arXiv:1510.02667
57. KEDR Collaboration, Phys. Lett. B **770**, 174 (2017). arXiv:1610.02827
58. A. Kurz, T. Liu, P. Marquard, M. Steinhauser, Phys. Lett. B **734**, 144 (2014). arXiv:1403.6400
59. J. Prades, E. de Rafael, A. Vainshtein, Adv. Ser. Direct. High Energy Phys. **20**, 303 (2009). arXiv:0901.0306
60. T. Aoyama, M. Hayakawa, T. Kinoshita, M. Nio, Phys. Rev. Lett. **109**, 111808 (2012). arXiv:1205.5370
61. A. Hoecker, W. Marciano, The muon anomalous magnetic moment. Review of Particle Physics, Particle Data Group. Phys. Rev. D **98**, 030001 (2018)
62. C. Gnendiger, D. Stökinger, H. Stökinger-Kim, Phys. Rev. D **88**, 053005 (2013). arXiv:1306.5546
63. M. Knecht, S. Peris, M. Perrottet, E. de Rafael, JHEP **11**, 003 (2002). arXiv:hep-ph/0205102
64. A. Czarnecki, W.J. Marciano, A. Vainshtein, Phys. Rev. D **67**, 073006 (2003). Erratum-ibid. D **73**, 119901 (2006). arXiv:hep-ph/0212229
65. R. Jackiw, S. Weinberg, Phys. Rev. D **5**, 2396 (1972)
66. W.J. Marciano, private communication (2019)
67. T. Ishikawa, N. Nakazawa, Y. Yasui, Phys. Rev. D **99**, 073004 (2019). arXiv:1810.13445
68. Muon *g*–2 Collaboration, Phys. Rev. D **73**, 072003 (2006). arXiv:hep-ex/0602035
69. F. Jegerlehner, EPJ Web Conf. **166**, 00022 (2018). arXiv:1705.00263
70. C. Sturm, Nucl. Phys. B **874**, 698 (2013). arXiv:1305.0581
71. Muon *g*–2 Collaboration, FERMILAB-DESIGN-2014-02 (2015).
72. BMW Collaboration, Phys. Rev. Lett. **121**, 022002 (2018). arXiv:1711.04980
73. HPQCD Collaboration (2019). arXiv:1902.04223
74. RBC and UKQCD Collaborations, Phys. Rev. Lett. **121**, 022003 (2018). arXiv:1801.07224
75. ETM Collaboration, JHEP **10**, 157 (2017). arXiv:1707.03019
76. ETM Collaboration, Phys. Rev. D 98, 114504 (2018). arXiv:1808.00887
77. ETM Collaboration, Phys. Rev. D **99**, 114502 (2019). arXiv:1901.10462
78. A. Gérardin et al., Phys. Rev. D **100**, 014510 (2019). arXiv:1904.03120
79. Sz. Borsanyi et al., arXiv:2002.12347
80. T. Blum et al., (2019). arXiv:1907.00864
81. M. Hoferichter et al., JHEP **10**, 141 (2018). arXiv:1808.04823